Limit-cycle oscillation of an elastic filament and caterpillar motion

Hidetsugu Sakaguchi
Department of Applied Science for Electronics and Materials, Interdisciplinary Graduate School of Engineering Sciences, Kyushu University, Kasuga, Fukuoka 816-8580, Japan

(Received 7 November 2008; revised manuscript received 15 January 2009; published 20 February 2009)

Soft biological materials can exhibit various active motion such as limit-cycle oscillation. The limit-cycle oscillation of active matter might be used for a mechanism of locomotion. We propose a simple model of an active elastic chain as an extension of the van der Pol equation. The uniform state is unstable, and exhibits a limit cycle of breathing motion. If the breathing motion is mirror symmetric, the elastic chain does not move as a whole. However, the breathing motion becomes a caterpillar motion and a unidirectional motion is induced, if an additional heterogeneity is involved or the chain is set on a spatially periodic sawtooth potential. We also analyze the model equation with coupled mode equations, and try to understand the bifurcation to the collective oscillation and the directional motion.

DOI: 10.1103/PhysRevE.79.026216 PACS number(s): 05.45.Xt, 46.40.−f, 87.19.lu

I. INTRODUCTION

Recently, self-organization and collective dynamics of active matter have been intensively studied. The collective motion appears in a large number of limit-cycle oscillators via mutual synchronization [1,2]. The collective motions of living organisms such as bacteria colonies, schools of fish, and flocks of flying birds have been studied from the viewpoint of dynamical systems and statistical mechanics [3,4]. A model including a number of neuro-oscillators was proposed to control bipedal locomotion [5]. Various active motions in biological materials have also been intensively studied. For example, an elastic model was proposed for helices of bacterial flagella [6]. The slow dynamics of the cytoskeleton was studied in the living cell [7].

Collective oscillations of soft elastic materials were observed in several systems. The self-oscillation was observed in gels [8]. Spontaneous oscillatory contraction was found in myofibril [9]. It is interesting that the oscillation occurs in the volume or the length of the elastic materials in these systems in contrast to general limit-cycle oscillators. Therefore, the self-oscillation of large deformation in the elastic materials can be applicable as soft mechanical devices such as microactuators and micropumps.

On the other hand, the ratchet motion has been intensively studied with respect to molecular motors [10,11]. Molecular motors are energy converters from chemical energy to mechanical energy. The ratchet mechanism is one method to generate a directional motion using thermal energy, chemical energy, or mechanical energy. There is a controversy with respect to a ratchet mechanism of the actin-myosin system in muscle contraction [12,13]. A directional motion of a droplet using a ratchet mechanism was experimentally demonstrated on a sawtooth potential by Linke *et al.* [14]. We studied a one-dimensional chain of Feynman ratchets, which exhibits a smooth directional motion [15].

In this paper, we propose a simple model of an active elastic chain as one of the simplest models of the self-oscillation of elastic materials. It is a simple extension of the van der Pol equation to an elastic chain. The uniform solution is unstable and exhibits a limit cycle of breathing motion. The breathing motion is mirror symmetric with respect to the center of mass, and therefore the elastic chain does not move as a whole. However, the breathing motion becomes a caterpillar motion, and a directional motion is induced by introducing some heterogeneity in the coupling strength or by setting the elastic chain on a spatially periodic sawtooth potential. That is, this model works as a deterministic ratchet. It is a mechanism to convert the energy of breathing motion into the energy of a directional motion.

II. MODEL EQUATION AND THE LIMIT-CYCLE OSCILLATION

The van der Pol equation is a typical model equation which exhibits the limit-cycle oscillation. It was originally proposed as a model equation for an electric oscillator including a vacuum tube. Here, the van der Pol equation is interpreted as a model for an elastic oscillator, which is written as

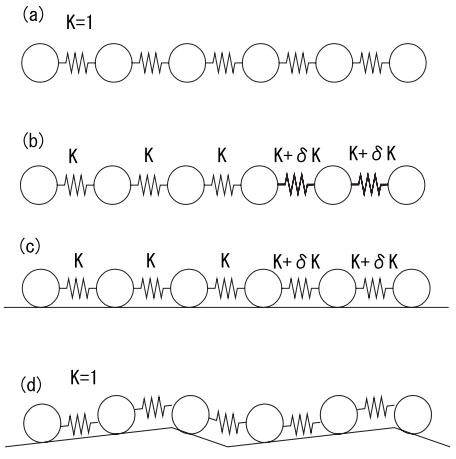

FIG. 1. Schematic figures of elastic chains (a) for Eq. (3) and Fig. 2, (b) for Eq. (7) and Fig. 3, (c) for Eq. (11) and Fig. 4, and (d) for Eq. (12) and Fig. 5.

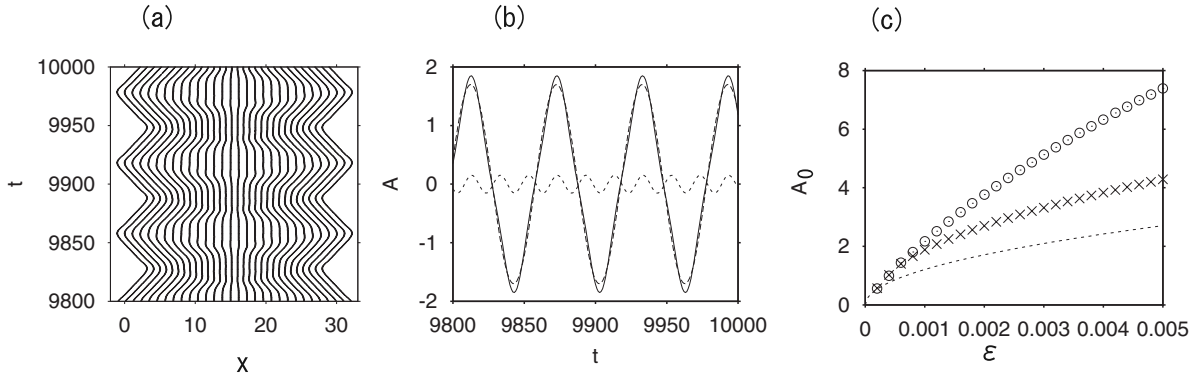

FIG. 2. (a) Time evolution of $x_i(t)$ for $\epsilon=0.001$ by Eq. (3). (b) Time evolutions by Eq. (4) of $A_1(t)$ (dashed curve with large amplitude), $A_3(t)$ (dashed curve with small amplitude), and $A_1(t)+A_3(t)$ (solid curve) for $\epsilon=0.001$. (c) Comparison of the amplitude of $x_N(t)$ by Eq. (3), $A_1(t)+A_3(t)$ by Eq. (4), and A_{10} by Eq. (6) as a function of ϵ.

$$\frac{d^2x}{dt^2} = (\epsilon - bx^2)\frac{dx}{dt} - Kx, \tag{1}$$

where x is the position of the oscillator, K denotes a spring constant, ϵ is a control parameter representing the distance from the instability point, and b is the coefficient of the nonlinear term. On the other hand, a simple model for a linear elastic chain is written as

$$\frac{d^2x_i}{dt^2} = K(x_{i+1} - 2x_i + x_{i-1}), \tag{2}$$

where x_i is the position of the ith elastic element and K is the coupling constant. We propose a simple model equation as a combination of Eqs. (1) and (2):

$$\frac{d^2x_i}{dt^2} = \{\epsilon - b(x_{i+1} - x_{i-1} - 2a)^2\}\frac{dx_i}{dt} + K(x_{i+1} - 2x_i + x_{i-1}), \tag{3}$$

where a is a natural length between the neighboring elements, and b is the coefficient of the nonlinear term. Figure 1(a) is a schematic figure for the elastic chain with $K=1$. The boundary conditions are assumed to be $x_{N+1}=x_N+a$ and $x_0=x_1-a$. It corresponds to the no-flux boundary conditions for the partial differential equation. If $\epsilon<0$, the system is stable, and x_i is located at the natural position $x_i=ia$. However, the stationary solution becomes unstable for $\epsilon>0$. The local deformation $x_{i+1}-x_{i-1}$ deviates from $2a$. If the local deformation $|x_{i+1}-x_{i-1}-2a|$ is larger than $\sqrt{\epsilon/b}$, the instability will be locally suppressed by the nonlinear term in Eq. (3).

In this paper, the parameters N, K, and b are set to be $N=30$, $K=1$, $b=1/4$, and $a=1$. Figure 2(a) shows time evolutions of $x_i(t)$ at $\epsilon=0.001$. The total length x_N-x_1 exhibits a limit-cycle oscillation. Even for the sufficiently small value of ϵ, a triangular-wave oscillation is observed. The period is $T=60$, which is close to $2N$.

The position $x_i(t)$ is approximately expressed by the Fourier transform as

$$x_i(t) = ia + \sum_{k=0}^{N-1} A_k \cos\{2\pi k(i-1)/N\},$$

owing to the no-flux boundary conditions. Since the breathing motion is mirror symmetric with respect to the center of mass, the Fourier amplitude A_k with even k is zero. If the Fourier amplitudes other than A_1 and A_3 are neglected, A_1 and A_3 obey coupled mode equations

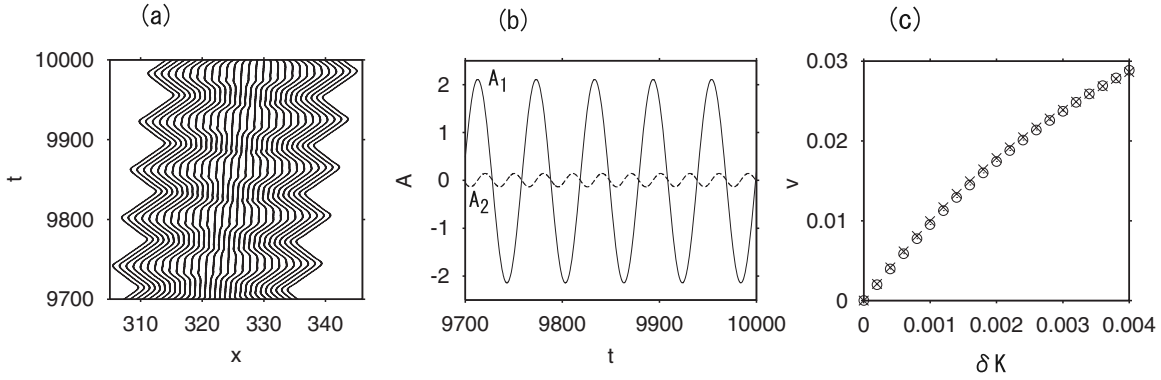

FIG. 3. (a) Time evolution of $x_i(t)$ for $\epsilon=0.001$, $F=0$, and $\delta K=0.003$. (b) Time evolutions by Eq. (3) of $A_1(t)$ (solid curve) and $A_2(t)$ (dashed curve) for $\epsilon=0.001$ and $\delta K=0.003$. (c) The average velocity v as a function of δK. The circles denote the results by direct numerical simulation, and the crosses denote the estimate by Eq. (9).

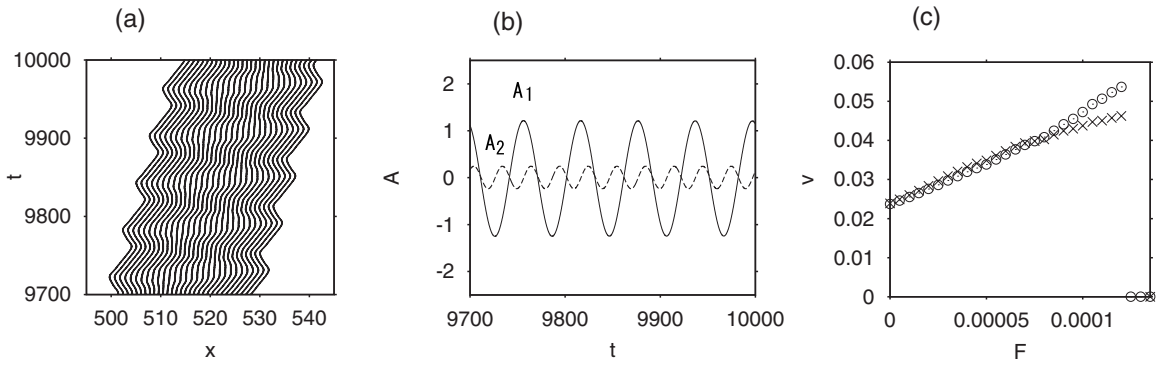

FIG. 4. (a) Time evolution of $x_i(t)$ for $\epsilon=0.001$, $F=0.0001$, and $\delta K=0.003$. (b) Time evolutions by Eq. (3) of $A_1(t)$ (solid curve) and $A_2(t)$ (dashed curve) for $\epsilon=0.001$, $F=0.0001$, and $\delta K=0.003$. (c) The average velocity v as a function of F. The circles denote the results by direct numerical simulation, and the crosses denote the estimate by Eq. (9).

$$\frac{d^2A_1}{dt^2} = \epsilon\frac{dA_1}{dt} - \omega_1^2 A_1 - bc_1^2A_1^2\left(\frac{dA_1}{dt} - \frac{dA_3}{dt}\right) - 2bc_3^2A_3^2\frac{dA_1}{dt} - 2bc_1c_3A_1A_3\frac{dA_1}{dt},$$

$$\frac{d^2A_3}{dt^2} = \epsilon\frac{dA_3}{dt} - \omega_3^2 A_3 - bc_3A_3^2\frac{dA_3}{dt} + bc_1^2A_1^2\frac{dA_1}{dt} - 2bc_1^2A_1^2\frac{dA_3}{dt}, \tag{4}$$

where $\omega_1=\sqrt{2\{1-\cos(\pi/N)\}}$, $\omega_3=\sqrt{2\{1-\cos(3\pi/N)\}}$, $c_1=\sin(\pi/N)$, and $c_3=\sin(3\pi/N)$. Note that the frequency $\omega_1 \sim \pi/N$ and therefore the period T is approximated at $2N$ for large N, and the natural frequency ω_3 for A_3 is close to $3\omega_1$. The Fourier modes A_1 and A_3 exhibit the Hopf bifurcation simultaneously at $\epsilon=0$ in Eq. (4). More generally, it can be shown that all the Fourier modes A_k's exhibit the Hopf bifurcation simultaneously at $\epsilon=0$ in the coupled mode equations including all the Fourier modes. It is a unique point in our model equation (3). Figure 2(b) shows time evolutions of $A_1(t)$, $A_3(t)$, and $A_1(t)+A_3(t)$ for $\epsilon=0.001$. The frequency locking of 1:3 takes place between the two modes A_1 and A_3 owing to the nonlinear terms in Eq. (4). The summation $A_1(t)+A_3(t)$ takes a triangular wave owing to the mutual enhancement of the peak structure. If the Fourier amplitude A_3 is further neglected, A_1 obeys the van der Pol equation

$$\frac{d^2A_1}{dt^2} = \epsilon\frac{dA_1}{dt} - \omega_1^2 A_1 - bc_1^2A_1^2\frac{dA_1}{dt}. \tag{5}$$

If $A_1=A_{10}\cos\omega_1 t$ is assumed, A_{10} is evaluated as

$$A_{10} = \frac{\sqrt{4\epsilon/b}}{\sin(\pi/N)}. \tag{6}$$

Figure 2(c) shows the amplitudes of the oscillatory time evolutions of $x_N(t)$ by Eq. (3), $A_1(t)+A_3(t)$ by Eq. (4), and A_{10} by Eq. (6). For sufficiently small ϵ, $x_N(t)$ by Eq. (3) can be approximated at $A_1(t)+A_3(t)$ by Eq. (5). When ϵ is sufficiently small, the oscillatory time evolution is well approximated at $A_1(t)+A_3(t)$. However, higher harmonics A_k with $k\geqslant 5$ is necessary and the approximation using only the two modes becomes worse, when ϵ is increased.

III. UNIDIRECTIONAL MOTION BY HETEROGENEITY

In this section, we consider a model including some heterogeneity in the coupling constant. The model equation is written as

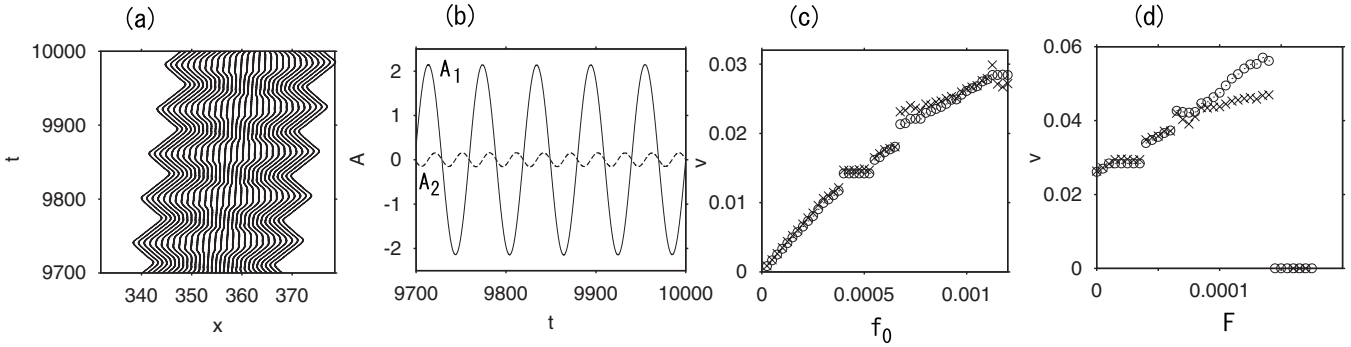

FIG. 5. (a) Time evolution of $x_i(t)$ for $\epsilon=0.001$, $F=0$, $\delta K=0$, and $f_0=0.001$. (b) Time evolutions of $A_1(t)$ (solid curve) and $A_2(t)$ (dashed curve) for $f_0=0.001$ and $F=0$. (c) Average velocity v as a function of f_0 for $F=0$. The circles denote the results by direct numerical simulation, and the crosses denote the estimate by Eq. (9). (d) Average velocity v as a function of F for $f_0=0.001$. The circles denote the results by direct numerical simulation, and the crosses denote the estimate by Eq. (9).

$$\frac{d^2x_i}{dt^2} = \{\epsilon - b(x_{i+1} - x_{i-1} - 2a)^2\}\frac{dx_i}{dt} + K(i+1/2)(x_{i+1} - x_i) - K(i-1/2)(x_i - x_{i-1}), \quad (7)$$

where $K(i+1/2)$ denotes the coupling constant between the ith and the $(i+1)$th elements. As shown schematically in Fig. 1(b), the coupling constant is slightly larger by δK near the the right end. In the numerical simulations, the coupling constant is set to be $K(i+1/2)=1$ for $i \leqslant 25$, and $K(i+1/2)=1+\delta K$ for $i \geqslant 26$. Figure 3(a) shows time evolutions of $x_i(t)$ for $\epsilon=0.001$ and $\delta K=0.003$. The mirror symmetry of the breathing motion is broken in this inhomogeneous system. A drift motion accompanying the breathing motion appears as a result of the asymmetry, which is similar to a caterpillar motion. There is a phase difference in the oscillations at the right and left ends.

Because the breathing motion is asymmetric, the Fourier amplitudes with even k appear in the coupled mode equations. Figure 3(b) displays time evolution of $A_1(t)$ and $A_2(t)$ calculated from the numerical result of the direct simulation of Eq. (3). That is, $A_1(t)$ and $A_2(t)$ are obtained from $A_k = (2/N)\Sigma_{j=1}^{N}(x_j - ja)\cos(2\pi k/N)$. From Fig. 3(b), $A_1(t)$ and $A_2(t)$ can be approximately expressed as $A_1(t) = 2.11\cos\{2\pi(t-9712.7)/60\}$ and $A_2(t) = 0.145\cos\{4\pi(t-9720.4)/60\}$. We can obtain coupled mode equations of A_0, A_1, and A_2 by neglecting all the other Fourier modes from Eq. (3). Then, $A_0(t)$ obeys the equation

$$\frac{d^2A_0}{dt^2} = \epsilon\frac{dA_0}{dt} - 2b(c_1^2A_1^2 + c_2^2A_2^2)\frac{dA_0}{dt} - 2bc_1c_2A_1A_2\frac{dA_1}{dt} + bc_1^2A_1^2\frac{dA_2}{dt}, \quad (8)$$

where $c_1=\sin(\pi/N)$ and $c_2=\sin(2\pi/N)$. The average velocity v of the drift motion of the elastic chain is approximated by the temporal average of dA_0/dt, because $A_0(t)$ represents the position of the center of mass. It is evaluated as

$$v = \frac{2bc_1c_2\langle A_1(t)A_2(t)(dA_2/dt)\rangle - bc_1^2\langle A_1(t)^2(dA_2/dt)\rangle}{\epsilon - 2bc_1^2\langle A_1(t)^2\rangle - 2bc_2^2\langle A_2(t)^2\rangle}, \quad (9)$$

where $\langle\cdots\rangle$ implies a temporal average. If $A_1(t) = A_{10}\cos\{\omega_1(t-t_1)\}$ and $A_2(t) = A_{20}\cos\{2\omega_1(t-t_2)\}$ are assumed, the average velocity v is calculated as

$$v = \frac{b\omega_1A_{10}^2A_{20}\sin\{2\omega_1(t_1-t_2)\}\{\sin^2(\pi/N) + \sin(\pi/N)\sin(2\pi/N)\}}{2\epsilon - 2b\{A_{10}^2\sin^2(\pi/N) + A_{20}^2\sin^2(2\pi/N)\}}. \quad (10)$$

The average velocity is therefore evaluated as $v=0.024$ from the approximation $A_1(t)=2.11\cos\{2\pi(t-9712.7)/60\}$ and $A_2(t)=0.145\cos\{4\pi(t-9720.4)/60\}$ for $\epsilon=0.001$ and $\delta K=0.003$, which is close to the numerical value 0.0237. Figure 3(c) shows the average velocity v as a function of ϵ. The circles denote the average velocity by the direct numerical simulation and the crosses denote the estimate by Eq. (9). Fairly good agreement implies that the directional motion is caused by the asymmetric breathing motion.

We can further include a Coulomb-type friction, which is a sliding friction with a solid surface, as shown schematically in Fig. 1(c). The model equation is written as

$$\frac{d^2x_i}{dt^2} = \{\epsilon - b(x_{i+1} - x_{i-1} - 2a)^2\}\frac{dx_i}{dt} + K(i+1/2)(x_{i+1} - x_i) - K(i-1/2)(x_i - x_{i-1}) - F\frac{dx_i/dt}{|dx_i/dt|}, \quad (11)$$

where F denotes the strength of the sliding friction. Figure 4(a) shows time evolutions of $x_i(t)$ for $\epsilon=0.001$ and $F=0.0001$. The coupling constant is set to be $K(i+1/2)=1$ for $i \leqslant 25$ and $K(i+1/2)=1+\delta K=1.003$ for $i \geqslant 26$, which is the same as the case of Fig. 3. As compared with Fig. 3(a), the average velocity v is larger owing to the effect of the sliding friction. It is interesting that the friction facilitates the directional motion. Figure 4(b) shows time evolutions of $A_1(t)$ and $A_2(t)$ for $\epsilon=0.001$ and $F=0.0001$. In contrast to Fig. 3(b), the amplitude of $A_1(t)$ decreases owing to the Coulomb friction. However, the amplitude of $A_2(t)$ and the phase difference $\omega_1(t_2-t_1)$ are larger than the case of $F=0$. As is predicted from Eq. (10), the increase of the amplitude of A_2 and the phase difference makes the average velocity increase. Figure 4(c) shows the average velocity v as a function of F for $\epsilon=0.001$ and $\delta K=0.003$. Actually, the average velocity increases with F. However, the breathing motion and then the caterpillar motion stop for $F > F_c=0.000125$. Near the threshold value F_c, the estimation by Eq. (9) for the average velocity becomes worse, where the higher harmonics is necessary.

IV. UNIDIRECTIONAL MOTION BY A RATCHET MECHANISM

In this section, we consider a drift motion on a spatially periodic sawtooth potential. The Coulomb friction is also included. The model equation is written as

$$\frac{d^2x_i}{dt^2} = \{\epsilon - b(x_{i+1} - x_{i-1} - 2a)^2\}\frac{dx_i}{dt} + K(x_{i+1} - 2x_i + x_{i-1}) - \frac{\partial U}{\partial x} - F\frac{dx_i/dt}{|dx_i/dt|}, \quad (12)$$

where $U(x)$ is a sawtooth potential with period L. We have

used a sawtooth potential $U(x)$, whose gradient is expressed as $-\partial U/\partial x=-f_0/3$ for $0<x_i<3L/4$ and $-\partial U/\partial x=f_0$ for $3L/4<x_i<L$. The parameter L is set to be $L=6$ for the numerical simulation, and the strength f_0 of the sawtooth potential is changed as a parameter. Figure 5(a) shows time evolutions of $x_i(t)$ for $\epsilon=0.001$, $K=1$, $F=0$, and $f_0=0.001$. The mirror symmetry of the breathing motion is broken by the sawtooth potential. A drift motion such as a caterpillar motion appears similarly to the previous model. Figure 5(b) shows time evolutions of $A_1(t)$ and $A_2(t)$ for $\epsilon=0.001$, $F=0$, and $f_0=0.001$. The Fourier mode $A_2(t)$ of even k $(k=2)$ is excited by the sawtooth potential. Figure 5(c) shows the average velocity v as a function of f_0. The circles denote the average velocity v by direct numerical simulation and the crosses denote the estimate by Eq. (9). Fairly good agreement is seen. The average drift velocity v increases with f_0; however, there are flat regions in the curve of $v(f_0)$ where $v(f_0)\sim$const. It might imply a spatial locking phenomenon. Figure 5(d) shows the average velocity v as a function of F at $f_0=0.001$. The average drift velocity increases with the coefficient F of the sliding friction until $F=F_c=0.00013$. For $F>F_c$, the breathing motion stops owing to the strong friction. It is interesting that the friction facilitates the caterpillar motion also in this model.

V. SUMMARY

We have found a breathing motion in a simple model of an active elastic filament. If the mirror symmetry of the breathing motion is broken, a directional motion similar to a caterpillar motion appears. The asymmetry has been introduced by a heterogeneity of the coupling strength or an external sawtooth potential. It is a mechanism to convert a part of the energy of the breathing motion into the energy of the directional motion. The Coulomb friction tends to enhance the directional motion. Our model can be interpreted as an example of deterministic ratchets. The model is also considered to be an example of self-organization of collective motion in a large number of active elements.

The model system was analyzed with the coupled mode equations. The simultaneous Hopf bifurcation of all the Fourier modes is a unique point in our model. As a result, not a sinusoidal oscillation but a triangular oscillation appears near the Hopf bifurcation. A drift motion occurs as a result of the appearance of the Fourier mode A_k of even k.

Our model is just a simple model constructed from a combination of the van der Pol equation and a linear elastic chain. The model might be too simple to apply to realistic elastic materials. It is necessary to elaborate the model in the future to apply to the oscillation in gel or myofibril.

[1] Y. Kuramoto, *Chemical Oscillations, Waves, and Turbulence* (Springer-Verlag, Berlin, 1984).
[2] A. Pikovskiy, M. Rosenblum, and J. Kurths, *Synchronization* (Cambridge University Press, Cambridge, 2001).
[3] T. Vicsek, A. Czirók, E. Ben-Jacob, I. Cohen, and O. Shochet, Phys. Rev. Lett. **75**, 1226 (1995).
[4] N. Shimoyama, K. Sugawara, T. Mizuguchi, Y. Hayakawa, and M. Sano, Phys. Rev. Lett. **76**, 3870 (1996).
[5] G. Taga, Y. Yamaguchi, and H. Shimizu, Biol. Cybern. **65**, 147 (1991).
[6] R. E. Goldstein, A. Goriely, G. Huber, and C. W. Wolgemuth, Phys. Rev. Lett. **84**, 1631 (2000).
[7] P. Bursac, G. Lenormand, B. Fabry, M. Oliver, D. A. Weitz, V. Viasnoff, J. P. Butler, and J. J. Fredberg, Nature Mater. **4**, 557 (2005).
[8] R. Yoshida, T. Takahasi, T. Yamaguchi, and H. Ichijo, J. Am. Chem. Soc. **118**, 5134 (1996).
[9] K. Yasuda, Y. Shindo, and S. Ishiwata, Biophys. J. **70**, 1823 (1996).
[10] F. Julicher, A. Ajdari, and J. Prost, Rev. Mod. Phys. **69**, 1269 (1997).
[11] P. Reimann, Phys. Rep. **361**, 57 (2002).
[12] R. D. Vale and F. Oosawa, Adv. Biophys. **26**, 97 (1990).
[13] Y. Y. Toyoshima, S. J. Kron, and J. A. Spudich, Proc. Natl. Acad. Sci. U.S.A. **87**, 7130 (1990).
[14] H. Linke, B. J. Alemán, L. D. Melling, M. J. Taormina, M. J. Francis, C. C. Dow-Hygelund, V. Narayanan, R. P. Taylor, and A. Stout, Phys. Rev. Lett. **96**, 154502 (2006).
[15] H. Sakaguchi, J. Phys. Soc. Jpn. **67**, 709 (1998).